Naftali (Tuli) Herscovici
Lincoln Laboratory - Group 61
Massachusetts Institute of Technology
244 Wood Street
Lexington, MA 02420-9108 USA
Tel: +1 (781) 981-0801
Fax: +1 (928) 832-4025
Skype/AOL: tuli01
Email: nherscovici@ll.mit.edu

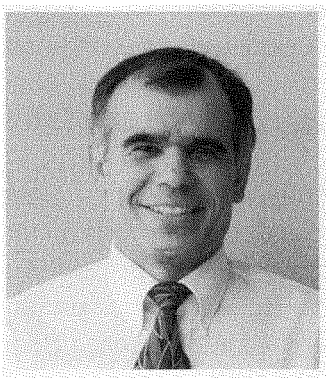

Christos Christodoulou
Department of Electrical and
Computer Engineering
University of New Mexico
Albuquerque, NM 87131-1356 USA
Tel: +1 (505) 277-6580
Fax: +1 (505) 277-1439
E-mail: christos@eece.unm.edu

Taking Advantage of Mutual Coupling in Radio-Communication Systems Using a Multi-Port Antenna Array

Frédéric Broydé and Evelyne Clavelier

Excem
12, chemin des Hauts de Clairefontaine, 78580 Maule, France
Tel: + 33 (0) 1 34 75 13 65; Fax: + 33 (0) 1 34 75 13 66; E-mail: fredbroyde@excem.fr, eclavelier@excem.fr

Abstract

This paper relates to the effect of mutual coupling in multi-port antenna arrays, such as those used in MIMO radio-communication systems. Approaches of different fields of electrical engineering are used to show that the interactions between antennas may improve performance. In particular, interesting properties may be obtained when the front end of a receiver is designed as a multiple-input-port and multiple-output-port device, as opposed to multiple independent single-input-port and single-output-port devices. The case of a receiver front end implementing a MIMO series-series feedback amplifier is presented in detail.

Keywords: MIMO communication systems; antenna arrays; amplifiers; amplifier noise; MIMO systems

1. Introduction

In a recent paper [1], Migliore observed that MIMO radio-communication systems are usually studied using the probabilistic communication approach. He then offered an intuitive presentation of MIMO radio-communication systems, from the perspective of electromagnetics. This approach invited us to question the relation between some common assumptions used in the probabilistic theory and the underlying physics. For instance, the performance of MIMO and other multi-antenna radio-communication systems is often assessed using the assumption of uncoupled channels. This is clearly an approximation, which fails if the antennas are close to each other. However, the physical size of the antenna array is often limited by the application, e.g., in the case of portable transceivers. There is consequently a need to review the effects of antenna separation in an array of antennas used as a multi-port, and how such effects may impact the properties of a radio-communication system and the design process.

The present paper is intended to be understandable by antenna and propagation specialists, telecommunication engineers, and RF front-end designers. It would ideally be a tutorial, if the field covered was more mature and all desirable results were available. The paper is better defined as an introduction to an active research area, based on the discussion of examples. The paper relates to a multi-port array of dipole antennas used for reception, shown in Figure 1. The paper discusses the effects of the interac-

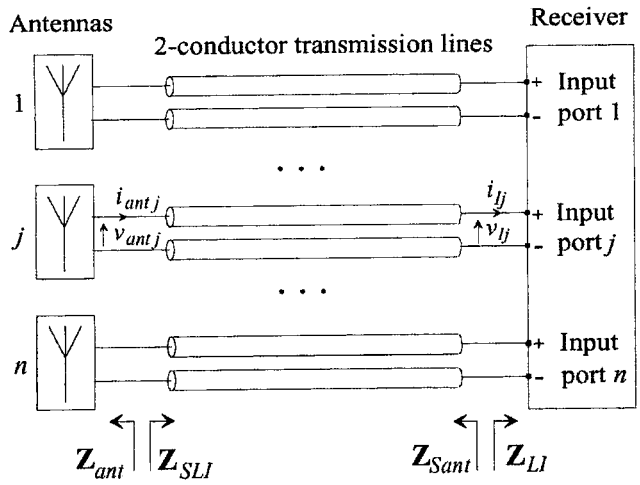

Figure 1. An array of n antennas connected to n uncoupled two-conductor transmission lines connected to a receiver having n input ports.

tions between antennas on the directivity pattern of each channel and on the correlations between voltages, for different types of items connected to the antennas. The purpose of this investigation is to show that a non-conventional radio-receiver front end may provide improved performance. Two types of non-conventional receiver front ends will be considered: passive and active, for which a detailed design example will be provided. A similar but shorter discussion applies to radio-transmitter front-end designs. Since the design of such non-conventional radio equipment is the result of the convergence of several technical fields, we have tried to present the facts in a manner that may sound convincing to engineers working in the different relevant fields. Unavoidably, specialists of different areas will find that parts of Section 2 are obvious.

The examples treated in this paper involve antennas, transmission lines, and circuits considered in the context of a deterministic plane wave impinging on the antenna array used for reception, or in the context of the probabilistic properties of a two-dimensional Rayleigh channel. We decided to use a single generic and flexible mathematical software program (*MathCAD®*), as opposed to multiple specialized programs (e.g., *NEC* for the antennas, *SPICE* for the circuits), which are not appropriate for the whole problem and would therefore require transfers of data relating to partial results. Additionally, each specialized tool would only be familiar – and hence convincing – to engineers of a single field. However, there are restrictions inherent in this possibility: we limit the discussion to academic arrays of dipole antennas, and the examples only cover antenna distances larger than 0.17λ.

2. Review of Concepts Applicable to Arrays of Antennas

This section provides basic results of antenna theory (Sections 2.1 and Appendix A), circuit theory (Section 2.2), telecommunication theory (Section 2.3 and Appendix B), and transmission-line theory (Section 2.4 and Appendix C).

2.1 The Impedance Matrix of an Array of Antennas

The components of the $n \times n$ impedance matrix $\mathbf{Z}_{ant}$ of an array of n antennas are the self- and mutual-impedances of an array of antennas [2, Chap. 10]. The impedance matrix is non-diagonal when the interactions between the antennas are non-negligible. The absolute values of the non-diagonal components of the impedance matrix are generally larger when the antennas are placed closer to each other.

The simple calculation of the impedance matrix of an array of dipole antennas presented in Appendix A and used below is based on the following approximations:

- The self impedance of an antenna of the array is computed as if the other antennas were not present, whereas it is clear that some currents will flow along such other antennas when they are left open-circuited;
- The mutual impedance between two antennas of the array is computed using a thin-antenna approximation;
- The mutual impedance between two antennas of the array is computed as if the other antennas were not present, whereas it is clear that some currents will flow along such other antennas when they are left open-circuited.

We note that according to such simplified calculations, the open-circuit voltages are the voltages in the absence of other array elements. This is a coarse approximation in which the mutual impedances are computed in a manner equivalent to using only one basis function in the Method of Moments [3]. The accuracy of this approximation is clearly improved when the distance between the antennas is increased.

Let us consider that our array of antennas is used for reception. Let j be an integer such that $1 \le j \le n$. We define the voltage between the terminals of the antenna j when the antenna array sees a linear multi-port load presenting an impedance matrix $\mathbf{Z}_{SLI}$ to be $v_{ant\,j}$, and the open-circuit voltage between the terminals of the antenna j when all antennas are left unconnected to be $v_{ant\,Oj}$. We also define the column vector of the voltages $v_{ant\,1},\ldots,v_{ant\,n}$ to be $\mathbf{V}_{ant}$, and the column vector of the voltages $v_{ant\,O1},\ldots,v_{ant\,On}$ to be $\mathbf{V}_{ant\,O}$. Of course, we have

$$\mathbf{V}_{ant} = \mathbf{Z}_{SLI}\left(\mathbf{Z}_{ant} + \mathbf{Z}_{SLI}\right)^{-1}\mathbf{V}_{ant\,O} = \left(\mathbf{1}_n + \mathbf{Z}_{ant}\mathbf{Z}_{SLI}^{-1}\right)^{-1}\mathbf{V}_{ant\,O}, \quad (1)$$

where $\mathbf{1}_n$ is the identity matrix of size $n \times n$. In the case where all components of the product of $\mathbf{Z}_{ant}$ by the inverse of $\mathbf{Z}_{SLI}$ have an absolute value much smaller than one, the interaction between the antennas is also small. In the opposite case, we have to consider that each component of $\mathbf{V}_{ant}$ is a linear combination of all the components of $\mathbf{V}_{ant\,O}$. Consequently, interference between these

contributions will occur: the directional pattern of each antenna used for reception will depend on $\mathbf{Z}_{SLI}$. From the reciprocity theorem, the directional pattern of a given antenna array used for reception, computed for a given $\mathbf{Z}_{SLI}$, is also the directional pattern of this antenna array used for emission, i.e., the radiation pattern, if $\mathbf{Z}_{SLI}$ is now the impedance matrix of a linear multi-port source seen by the antenna array.

2.2 Hermitian Matching and Maximum Power Transfer

We use ${}^{t}\mathbf{X}$ to denote the transpose of a matrix $\mathbf{X}$, $\overline{\mathbf{X}}$ to denote the complex conjugate of $\mathbf{X}$, and $\mathbf{X}^{*} = {}^{t}\overline{\mathbf{X}}$ to denote the Hermitian adjoint of $\mathbf{X}$. Since the antenna array will always radiate some power if it is connected to generators, $\mathbf{Z}_{ant} + \mathbf{Z}_{ant}^{*}$ is positive definite. Desoer [4, 5] proved that for given $\mathbf{V}_{antO}$ and $\mathbf{Z}_{ant}$, the set of $\mathbf{Z}_{SLI}$ drawing maximum average power from the array of antennas is defined by the equation

$$\mathbf{Z}_{SLI}\left(\mathbf{Z}_{ant}+\mathbf{Z}_{ant}^{*}\right)^{-1}\mathbf{V}_{antO} = \mathbf{Z}_{ant}^{*}\left(\mathbf{Z}_{ant}+\mathbf{Z}_{ant}^{*}\right)^{-1}\mathbf{V}_{antO} \tag{2}$$

and is consequently an $n(n-1)$-dimensional subspace of the n^2 dimensional vector space of complex $n \times n$ matrices.

When the array of antennas is used for reception, $\mathbf{V}_{antO}$ depends on the angles of incidence of the impinging wave. Among all the maximizing impedance matrices $\mathbf{Z}_{SLI}$, we may choose $\mathbf{Z}_{ant}^{*}$, which is independent of $\mathbf{V}_{antO}$, and this choice is the only impedance matrix that maximizes power transfer for any arbitrary $\mathbf{V}_{antO}$. By definition, a multi-port load connected to the antennas provides Hermitian matching if $\mathbf{Z}_{SLI} = \mathbf{Z}_{ant}^{*}$ (Hermitian matching at the near end) or if $\mathbf{Z}_{LI} = \mathbf{Z}_{Sant}^{*}$ (Hermitian matching at the far end). We may therefore state that an antenna array used for receiving radio signals delivers maximum power when a Hermitian matching is provided. In other words, Hermitian matching is a sufficient condition for maximum-power transfer. Let us mention that if no nonreciprocal devices are used in the array of antennas, $\mathbf{Z}_{ant}$ is a symmetrical matrix, and the Hermitian adjoint of $\mathbf{Z}_{ant}$ is equal to the matrix complex conjugate of $\mathbf{Z}_{ant}$.

2.3 Correlation Coefficients of the Voltages

Let i and j be integers greater than or equal to one and less than or equal to n. If we use $\overline{x}$ to denote the complex conjugate of a complex number x, the covariance between the complex voltages delivered by antennas number i and j of the array of antennas is $\left\langle v_{anti}\overline{v_{antj}}\right\rangle$, and the covariance between the complex open-circuit voltages across these antennas number i and j is $\left\langle v_{antOi}\overline{v_{antOj}}\right\rangle$. Consequently, $\left\langle \mathbf{V}_{ant}\mathbf{V}_{ant}^{*}\right\rangle$ is the $n \times n$ covariance matrix of the antenna voltages, and $\left\langle \mathbf{V}_{antO}\mathbf{V}_{antO}^{*}\right\rangle$ is the covariance matrix of the open-circuit antenna voltages. We can easily establish [6] that

$$\left\langle \mathbf{V}_{ant}\,\mathbf{V}_{ant}^{*}\right\rangle = \mathbf{Z}_{SLI}\left(\mathbf{Z}_{SLI}+\mathbf{Z}_{ANT}\right)^{-1}\left\langle \mathbf{V}_{antO}\,\mathbf{V}_{antO}^{*}\right\rangle\left(\mathbf{Z}_{SLI}+\mathbf{Z}_{ANT}\right)^{-1*}\mathbf{Z}_{SLI}^{*}. \tag{3}$$

We will assume that the antennas are only sensitive to the vertical electric fields, E_z, occurring in a given horizontal plane, like vertical dipoles having their respective electrical centers on this plane. Although this is only an approximation as explained in Section 2.1, we will also assume that the open-circuit condition corresponds to a lack of interaction between the antennas.

The covariances may be computed using additional assumptions. We will consider a fixed receiver in a scattering-rich environment. More precisely, if we assume two-dimensional Rayleigh channels, $\left\langle v_{antOi}\overline{v_{antOj}}\right\rangle$ is the covariance between the vertical electric fields, E_z, at the electrical centers of the antennas, multiplied by the effective heights, $H_{eff\,i}$ and $H_{eff\,j}$ of the antennas i and j for the zenith angle of incidence $\theta = \pi/2$ (see Appendix A). We can then use the result of Appendix B on the covariance between the vertical electric fields to obtain

$$\left\langle v_{antOi}\overline{v_{antOj}}\right\rangle = \left\langle |E_z|^2\right\rangle H_{eff\,i}\overline{H_{eff\,j}}\,\mathrm{J}_0\left(kd_{ij}\right), \tag{4}$$

where J_0 is the Bessel function of the first kind of order 0, k is the wavenumber, and d_{ij} is the distance between antennas number i and j having the same coordinate, z. The corresponding correlation coefficients are

$$r_{ij} = \frac{\left\langle v_{antOi}\overline{v_{antOj}}\right\rangle}{\sqrt{\left\langle |v_{antOi}|^2\right\rangle\left\langle |v_{antOj}|^2\right\rangle}} = \frac{H_{eff\,i}\overline{H_{eff\,j}}}{|H_{eff\,i}||H_{eff\,j}|}\mathrm{J}_0\left(kd_{ij}\right). \tag{5}$$

In the case where the antennas are identical,

$$r_{ij} = \frac{\left\langle v_{antOi}\overline{v_{antOj}}\right\rangle}{\sqrt{\left\langle |v_{antOi}|^2\right\rangle\left\langle |v_{antOj}|^2\right\rangle}} = J_0\left(kd_{ij}\right). \tag{6}$$

2.4 A Set of Two-Conductor Interconnections

As shown in Figure 1, each antenna of the antenna array may be connected to the front end of a multi-port receiver using a two-conductor interconnection. The impedance matrix, $\mathbf{Z}_{SLI}$, seen by the array of antennas looking into the near ends of such interconnections is a consequence of the characteristics of the interconnections and of the impedance matrix, $\mathbf{Z}_{LI}$, of the multi-port con-

nected to the far ends. Also, the impedance matrix, $\mathbf{Z}_{Sant}$, seen by this multi-port looking into the far ends of the interconnections is a consequence of the characteristics of the interconnections and of the impedance matrix $\mathbf{Z}_{ant}$. The computation of $\mathbf{Z}_{SLI}$, $\mathbf{Z}_{Sant}$, and the voltages, v_{Lj}, across a port of the multi-port is covered in Appendix C.

Since the characteristic impedance matrix, $\mathbf{Z}_C$, of the uncoupled interconnections, defined by Equation (37) of Appendix C, is diagonal and $\mathbf{Z}_{ant}$ is not diagonal, it is not possible to achieve image matching, i.e., $\mathbf{Z}_C = \mathbf{Z}_{ant}$ (in the literature on antennas and transmission lines, "matching" refers to image matching). However, it is often possible to achieve Hermitian matching (see Section 3.3).

3. An Example of a Linear Array of Three Loosely Coupled Dipole Antennas

This section applies to a first linear array of three parallel half-wave dipole antennas (side-by-side configuration) for 433 MHz, presenting a $\lambda/2 = 346\,\text{mm}$ spacing between the nearest array elements. The impedance matrix of the antenna array is computed as

$$\mathbf{Z}_{ant} = \begin{pmatrix} 73.1 & -12.5-29.9j & 4.0+17.7j \\ -12.5-29.9j & 73.1 & -12.5-29.9j \\ 4.0+17.7j & -12.5-29.9j & 73.1 \end{pmatrix} \Omega, \quad (7)$$

using the approach described in Section 2.1. When the antenna array is not connected to anything, the open-circuit voltage is equal to the effective height, H_{eff}, given by Equation (26), and independent from the azimuth, φ. For a zenith angle $\theta = \pi/2$, this effective height is 220 mm, and the matrix of the correlation coefficients, r_{ij}, of open-circuit voltages given by Equation (6) is

$$(r_{ij}) = \begin{pmatrix} 1.000 & -0.304 & 0.220 \\ -0.304 & 1.000 & -0.304 \\ 0.220 & -0.304 & 1.000 \end{pmatrix}. \quad (8)$$

Let us now see how this antenna array behaves in two different applications.

3.1 The Case of a Conventional Front-End Design

Let us assume that the antenna array is used for reception, and implemented in the conventional scheme shown in Figure 2. The analog processing and conversion circuits used in Figure 2 may implement the following main steps: frequency conversion, filtering and amplification of the intermediate-frequency signal, and demodulation and analog-to-digital conversion of the I and Q signals. For example, the multiple-input signal-processing device used in Figure 2 may implement the following main steps: OFDM demodulation of each input signal, space-time decoding (MIMO decoding), channel decoding, and source decoding [7-9].

In Figure 2, we note that the front end of the receiver – comprising the bandpass filters, the low-noise amplifiers (LNAs), and the RF part of the analog-processing and conversion circuits – is made of multiple independent single-input-port and single-output-port devices. Consequently, the impedance matrix, $\mathbf{Z}_{SLI}$, seen by the array of antennas is diagonal.

For instance, let us assume that the antenna array sees uncoupled scalar loads of 73.0 Ω, i.e.,

$$\mathbf{Z}_{SLI} = \begin{pmatrix} 73.0 & 0.0 & 0.0 \\ 0.0 & 73.0 & 0.0 \\ 0.0 & 0.0 & 73.0 \end{pmatrix} \Omega. \quad (9)$$

The column vector, $\mathbf{V}_{ant}$, of the antenna voltage may be computed using Equation (1), which shows that each antenna voltage, $v_{ant\,j}$, is now a linear combination of all open-circuit antenna voltages, $v_{ant\,O1}, \ldots, v_{ant\,On}$. The resulting interferences renders the antenna voltages azimuth dependent. Figure 3 shows the corresponding directivity pattern. Note that in the same field, a single dipole antenna in free space would deliver 83 μW to a 73.0 Ω load. Using Equation (3), we can compute the correlation coefficients, r_{ij}, of antenna voltages, and get

$$(r_{ij}) = \begin{pmatrix} 1.000 & -0.116-0.012j & 0.108 \\ -0.116+0.012j & 1.000 & -0.116+0.012j \\ 0.108 & -0.116-0.012j & 1.000 \end{pmatrix}. \quad (10)$$

The absolute values of the correlation coefficients are slightly reduced by antenna loading. This is somewhat surprising, since according to our model, the loading creates the interaction between the antennas, and interactions usually cause correlation. However, the decorrelation of the received signal by mutual coupling of the antennas is an established phenomenon [6], although we will show in Section 4.1 that it does not always occur.

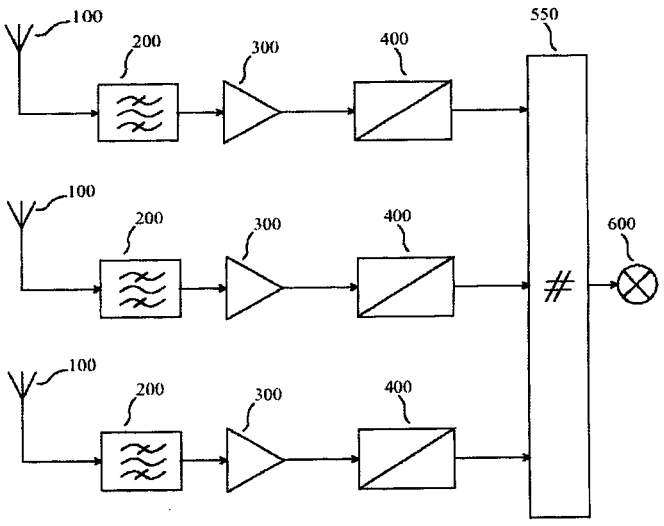

Figure 2. A conventional three-antenna receiver for MIMO radio transmission comprises three antennas (100), three bandpass filters (200), three low-noise amplifiers (300), three analog-processing and conversion circuits (400), and a multiple-input signal-processing device (550), the output of which is connected to the destination (600).

3.2 The Case of a MIPMOP Front-End Design

We will refer to any multiple-input-port receiver front end (or multiple-output-port transmitter front end) as a multiple-input port and multiple-output port (MIPMOP) front end if it is made not only of multiple-independent single-input-port and single-output-port devices. The block diagram of a MIMO receiver using such a MIPMOP front end is shown in Figure 4, in which the front end comprises a MIPMOP passive linear matching network, the low-noise amplifier, and the RF part of the analog-processing and conversion circuits. The MIPMOP passive linear matching network used in Figure 4 may be such that Hermitian matching is obtained between $\mathbf{Z}_{ant}$ and $\mathbf{Z}_{SLI}$. In this case, Figure 5 shows the corresponding directivity pattern in the configuration used for Figure 3. We note that the characteristics shown in Figure 5 do not significantly differ from those shown in Figure 3. The matrix of the correlation coefficients, r_{ij}, of antenna voltages is

$$\left(r_{ij}\right)=\begin{pmatrix} 1.000 & -0.307-0.028j & 0.313 \\ -0.307+0.028j & 1.000 & -0.307+0.028j \\ 0.313 & -0.307-0.028j & 1.000 \end{pmatrix}. \tag{11}$$

3.3 Effect of Interconnections

Some sort of interconnection is needed to link each antenna of the array to a receiver. For instance, let us consider that the antennas are connected to the receiver using three 0.346-m-long cables having propagation velocities of $0.659c_0$, characteristic impedances of 75 Ω (close to the diagonal elements of $\mathbf{Z}_{ant}$), and attenuations of 0.29 dB/m, all at 433 MHz. The impedance matrix, $\mathbf{Z}_{Sant}$, seen by the receiver may be computed using Equations (7) and Equation (45) of Appendix C. We find that

$$\mathbf{Z}_{Sant}=\begin{pmatrix} 69.1+11.1j & 11.2+22.4j & -9.5-7.6j \\ 11.2+22.4j & 69.1+11.1j & 11.2+22.4j \\ -9.5-7.6j & 11.2+22.4j & 69.1+11.1j \end{pmatrix}\Omega. \tag{12}$$

We note that $\mathbf{Z}_{Sant}$ is very different from $\mathbf{Z}_{ant}$. If the receiver presents an impedance matrix $\mathbf{Z}_{LI}$ equal to $\mathbf{Z}_{Sant}^{*}$, we obtain Hermitian matching between the far end of the cable and the receiver. Using Equations (7) and (41), we can also compute the impedance matrix, $\mathbf{Z}_{LI}$, of the receiver that would produce a Hermitian matching between the antenna array and the near end of the cable, i.e., $\mathbf{Z}_{SLI}^{*}=\mathbf{Z}_{ant}$. We find

$$\mathbf{Z}_{LI}=\begin{pmatrix} 68.2-12.5j & 11.7-24.3j & -10.4+8.1j \\ 11.7-24.3j & 68.2-12.5j & 11.7-24.3j \\ -10.4+8.1j & 11.7-24.3j & 68.2-12.5j \end{pmatrix}\Omega. \tag{13}$$

We note that Equation (13) is not exactly the Hermitian adjoint of Equation (12). It can be shown that this is a consequence of losses: if lossless cable had been used, we would have obtained $\mathbf{Z}_{LI}=\mathbf{Z}_{Sant}^{*}$.

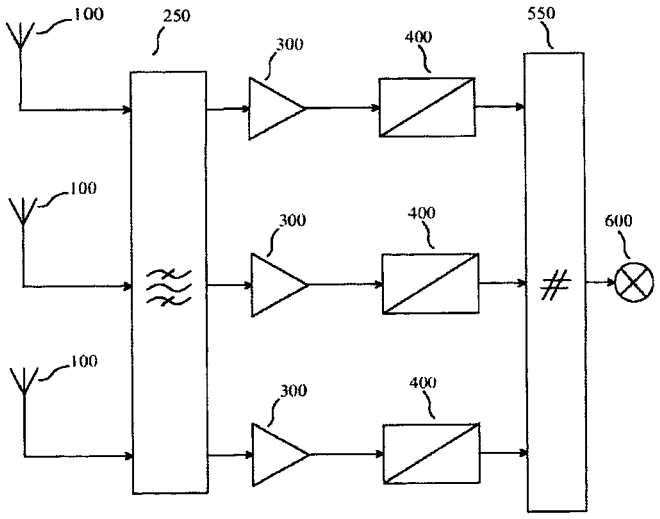

Figure 4. A three-antenna receiver for MIMO radio transmission using a MIPMOP front end may, for instance, comprise three antennas (100), a MIPMOP passive linear matching network (250), and the other blocks mentioned in Figure 2.

4. An Example of a Circular Array of Six Tightly Coupled Dipole Antennas

This section applies to a circular array of six parallel half-wave dipole antennas (side-by-side configuration) for 1880 MHz, presenting a $0.17\lambda = 27$ mm spacing between the nearest array elements. The impedance matrix of the antenna array is computed as

$$\mathbf{Z}_{ant}=\begin{pmatrix} 73.1 & 57.0-12.2j & 30.5-33.9j & 19.8-37.0j & 30.5-33.9j & 57.0-12.2j \\ 57.0-12.2j & 73.1 & 57.0-12.2j & 30.5-33.9j & 19.8-37.0j & 30.5-33.9j \\ 30.5-33.9j & 57.0-12.2j & 73.1 & 57.0-12.2j & 30.5-33.9j & 19.8-37.0j \\ 19.8-37.0j & 30.5-33.9j & 57.0-12.2j & 73.1 & 57.0-12.2j & 30.5-33.9j \\ 30.5-33.9j & 19.8-37.0j & 30.5-33.9j & 57.0-12.2j & 73.1 & 57.0-12.2j \\ 57.0-12.2j & 30.5-33.9j & 19.8-37.0j & 30.5-33.9j & 57.0-12.2j & 73.1 \end{pmatrix}, \tag{14}$$

using the approach described in Section 2.1. For a zenith angle $\theta=\pi/2$, the open-circuit voltages are 51 mV for an incident field of 1 V/m. The matrix of the correlation coefficients, r_{ij}, of the open-circuit voltages is

$$\left(r_{ij}\right)=\begin{pmatrix} 1.000 & 0.734 & 0.311 & 0.146 & 0.311 & 0.734 \\ 0.734 & 1.000 & 0.734 & 0.311 & 0.146 & 0.311 \\ 0.311 & 0.734 & 1.000 & 0.734 & 0.311 & 0.146 \\ 0.146 & 0.311 & 0.734 & 1.000 & 0.734 & 0.311 \\ 0.311 & 0.146 & 0.311 & 0.734 & 1.000 & 0.734 \\ 0.356 & 0.311 & 0.146 & 0.311 & 0.734 & 1.000 \end{pmatrix}. \tag{15}$$

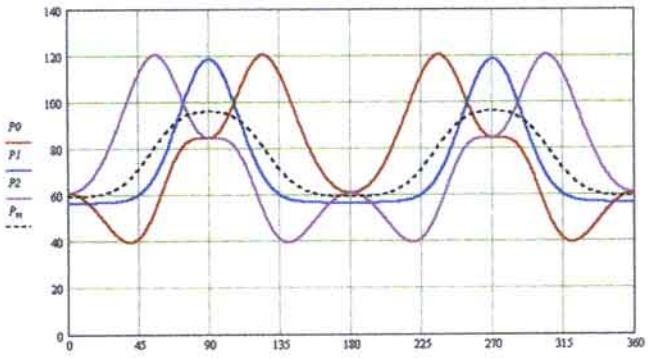

Figure 3. The average powers $P0$, $P1$, and $P2$, delivered by each antenna (in μW), and the mean, $P_M = (P0+P1+P2)/3$ of the average powers as a function of the azimuth angle φ (in degrees) for a conventional front-end design receiving an incident plane wave of 1 V/m (peak) and for $\theta = \pi/2$.

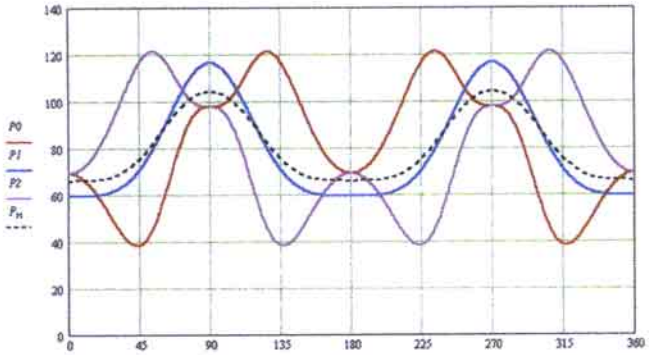

Figure 5. The average powers $P0$, $P1$, and $P2$, delivered by each antenna (in μW), and the mean $P_M = (P0+P1+P2)/3$ of the average powers as a function of the azimuth angle φ (in degrees) for a MIPMOP front-end design providing Hermitian matching to the antenna array receiving an incident plane wave of 1 V/m (peak) and for $\theta = \pi/2$.

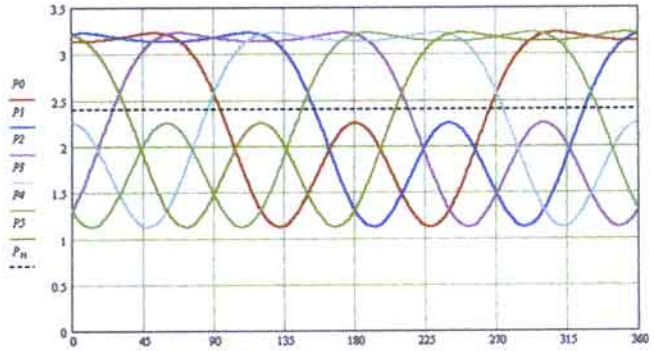

Figure 6. The average powers $P0$, $P1$, $P2$, $P3$, $P4$, and $P5$, delivered by each antenna (in μW), and the mean, P_M, of the average powers as a function of the azimuth angle φ (in degrees) for a conventional front-end design receiving an incident plane wave of 1 V/m (peak) and for $\theta = \pi/2$.

Figure 10. The average powers $P0$, $P1$, $P2$, and $P3$, delivered by the outputs of the MIPMOP amplifier shown in Figure 8 (in μW) and the mean, P_M, of the average powers as a function of the azimuth angle φ (in degrees) when an antenna array receives an incident plane wave of 1 V/m (peak) with $\theta = \pi/2$.

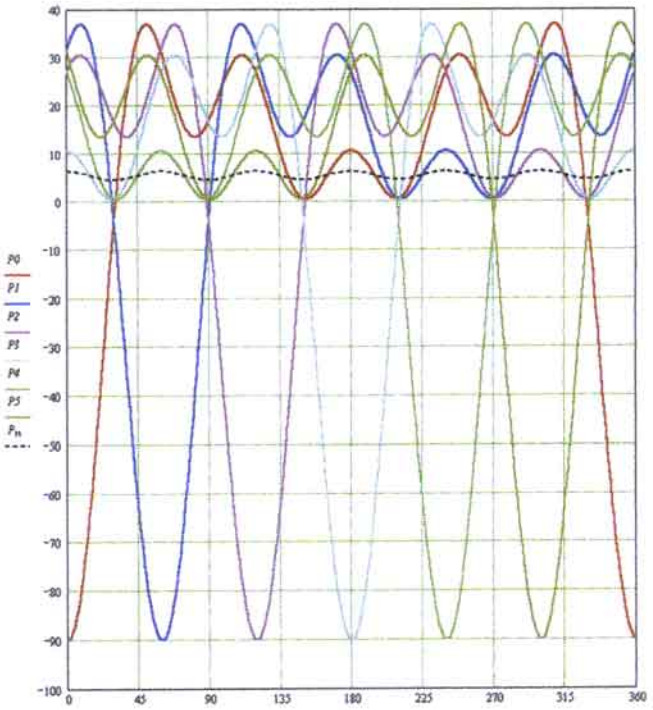

Figure 7. The average powers $P0$, $P1$, $P2$, $P3$, $P4$, and $P5$, delivered by each antenna (in μW), and the mean, P_M, of the average powers as a function of the azimuth angle φ (in degrees) for a MIPMOP front-end design providing Hermitian matching to the antenna array receiving an incident plane wave of 1 V/m (peak) and for $\theta = \pi/2$.

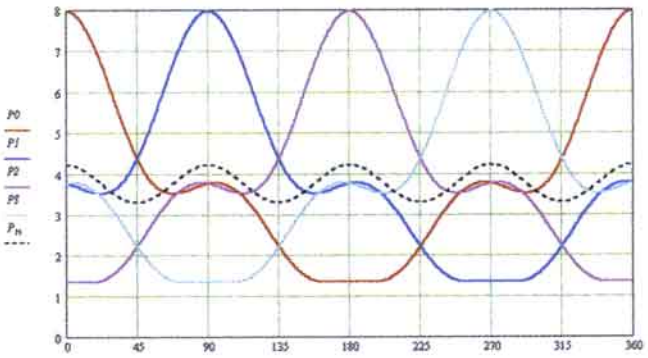

Figure 9. The average powers $P0$, $P1$, $P2$, and $P3$, delivered by each antenna (in μW), and the mean, P_M, of the average powers as a function of the azimuth angle φ (in degrees) for a conventional front-end design receiving an incident plane wave of 1 V/m (peak) and for $\theta = \pi/2$.

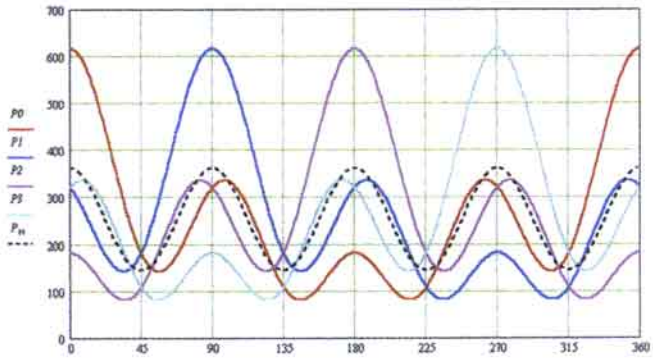

We will now examine how this antenna array behaves in the two configurations considered in Section 3.

4.1 The Case of a Conventional Front-End Design

In the case where the antenna array sees six uncoupled scalar loads of 73.0 Ω, we obtain the directivity pattern shown in Figure 6. The mean of the average powers is practically independent of the angle of arrival, and close to 2.4 μW. Consequently, the antenna array delivers about 14.4 μW irrespective of the azimuth angle φ, whereas in the same field, a single dipole antenna in free space would deliver 4.4 μW to a 73.0 Ω load. Using Equation (3), we can compute the correlation coefficients, r_{ij}, of the antenna voltages, and get

$$\left(r_{ij}\right)=\begin{pmatrix} 1.000 & 0.356 & -0.250 & -0.261 & -0.250 & 0.356 \\ 0.356 & 1.000 & 0.356 & -0.250 & -0.261 & -0.250 \\ -0.250 & 0.356 & 1.000 & 0.356 & -0.250 & -0.261 \\ -0.261 & -0.250 & 0.356 & 1.000 & 0.356 & -0.250 \\ -0.250 & -0.261 & -0.250 & 0.356 & 1.000 & 0.356 \\ 0.356 & -0.250 & -0.261 & -0.250 & 0.356 & 1.000 \end{pmatrix}. \quad (16)$$

The absolute value of four correlation coefficients in each row (or column) is significantly reduced by antenna loading, but one correlation coefficient in each row (or column) is increased. Consequently, we can say that decorrelation of a received signal by mutual coupling (proven in [6] between two identical antennas) does not fully apply between all antenna pairs of an array of three or more antennas.

4.2 The Case of a MIPMOP Front-End Design

In the case of a receiver using a MIPMOP front end providing Hermitian matching between $\mathbf{Z}_{ant}$ and $\mathbf{Z}_{SLI}$, Figure 7 shows the power delivered by each antenna and the average power as a function of the azimuth, in the configuration used for Figure 6. We note that the characteristics shown in Figure 3 are very different from those shown in Figure 6. The average power slightly depends on the angle of arrival, and is about twice higher than in Figure 6. An interesting feature is that the sign of the power delivered by each antenna depends on the direction of arrival: a lot of active power is exchanged between the antennas. In summing the power delivered by each antenna, cancellation occurs, and a total power ranging from 27 μW to 37 μW is delivered to the load. The large exchange of power suggests that low losses in the antenna and in the MIPMOP passive linear matching network are important in obtaining the performance shown in Figure 7.

5. The Interest in a MIPMOP Front-End Design in a Receiver

Can we take advantage of mutual coupling in a receiver using multiple antennas? In other words, we wonder whether well-designed MIPMOP front ends are better than conventional multiport receiver front ends. Here, two issues must be considered: the directional pattern of each channel at the output of the front end, and the signal-to-noise ratio. In the case of a conventional front-end design, the correlation at the output of the front end corresponds to the correlation coefficients of the antenna voltages shown in Equations (10) and (16). However, in the case of an MIMOP front-end design, the correlation at the output of the front end does not correspond to the correlation coefficients of the antenna voltages shown in Equation (11).

The directional patterns are related to signal correlation. Several authors [10-12] have investigated the effect of a passive lossless MIPMOP network providing Hermitian matching to its antenna ports and Hermitian matching to uncoupled scalar loads at its output (bilateral Hermitian matching). They came to the conclusion that bilateral Hermitian matching can be used for advanced beam-forming, and that the output voltages always have a correlation of zero for nonzero spacing (in the case of two-dimensional Rayleigh channels) because the matching network modifies the directional patterns of the n channels such that they are orthogonal over the azimuth. In fact, the orthogonality of the patterns of any lossless decoupled and matched antenna system was previously proven by Stein [13]. The decorrelation effect is beneficial, but not necessarily essential, since correlation coefficients lower than 0.6 are usually considered to be sufficiently low for good diversity action [6, 8].

Hermitian matching to the array of antennas will directly provide a stronger signal because of maximum power transfer. Such matching might eventually improve the signal-to-noise ratio of a MIPMOP front-end, if noise is not degraded by the provision made for obtaining conjugate matching. For instance, let us consider the scheme shown in Figure 4. If the MIPMOP passive linear matching network provides bilateral Hermitian matching, the low-noise amplifier and the analog-processing and conversion circuits may be identical to those used in Figure 2, and may operate under the same conditions. In this case, a degradation of the noise performance may be only the result of losses inherent to a practical implementation of the passive MIPMOP network. In this respect, one can show that a reciprocal, lossless network providing bilateral Hermitian matching exists. However, this theoretical result says nothing about a typical circuit diagram that could be used to assess achievable losses. This question was addressed by Weber et al [14, 15]: the matching network is very complex (it comprises $n(2n+1)$ circuit elements), and losses must be taken into account to obtain a realistic design, as hinted at in Section 4.2.

In a single-input-port single-output-port amplifier, the source impedance Z_{opt} that results in the minimum noise figure is usually not the impedance corresponding to conjugate matching with the input impedance of the amplifier. However, it is possible to design a low-noise amplifier in which Z_{opt} takes on a prescribed value, such that the minimum noise figure and conjugate matching are simultaneously achieved [16, 17]. If such low-noise amplifiers are used in Figure 4, a MIPMOP passive linear matching network providing bilateral Hermitian matching will also provide optimized noise performance. More generally, a MIPMOP-front end can be designed to provide the best signal-to-noise ratios at its n outputs. However, we will not address this question here, since it would require an accurate definition of the quantity to be optimized, and an involved development.

6. The Interest in a MIPMOP Front-End Design in a Transmitter

Can we take advantage of mutual coupling in a transmitter using multiple antennas? If we consider a passive lossless MIPMOP network having n antenna ports connected to the antenna and n input ports connected to the outputs of n uncoupled power amplifiers, we need to consider the radiation patterns and the radiation efficiency.

In the case of a transmitter, the radiation pattern for each channel can be modeled at will, regardless of antenna coupling, by suitable digital processing prior to the digital-to-analog conversion preceding power amplification. Such beam forming is more effective in a transmitter than in a receiver, since noise is not an issue (in the case of a transmitter, the main limit is the resolution of the digital-to-analog converters). Completely decorrelated beams may be obtained in this manner [18].

The radiation efficiency, i.e., the ratio of the radiated power to the total power flowing out of the power amplifiers, is not governed by some sort of matching of the power amplifier to the antennas. For instance, in the case of a transmitter connected to a single antenna, the impedance of the antenna is not matched to the output of the power amplifier. The output filter or matching circuit of the transmitter is merely designed to present to the active device(s) a load impedance producing optimum performance for the desired output power and operating class [19, Sec. 4.7; 20, Chap. VI; 21, Chap. 9]. This is further justified by two additional facts: power amplifiers are often not linear (depending on the class of operation), and no power is supposed to flow from the antenna to the power amplifier in the case of a transmitter connected to a single antenna.

If we now come back to the case of a transmitter having n output ports connected to an array of antennas, let us consider the effect of having the power amplifiers see a non-diagonal impedance matrix: in this case, a current injected by the power amplifier i produces a voltage at the output of the power amplifier j. This voltage will produce losses, distortion, cross-modulation, and increased device stress in the amplifier j. This voltage might even produce anomalous operation in a switched-mode power amplifier (e.g., class E or F). Radiation efficiency will consequently be improved and the other detrimental phenomena will be avoided if a passive low-loss MIPMOP circuit, inserted between the antenna terminals and the power-amplifier outputs, is such that the power amplifiers see a diagonal impedance matrix. This requirement is far less stringent than bilateral Hermitian matching, but such networks are nevertheless likely to be complex and significantly lossy when n is large.

7. An Active MIPMOP Front End for a Receiver

In Section 5, we found that a MIPMOP receiver front-end design could provide better performance than a conventional design. We also mentioned that a passive matching network, providing Hermitian matching to the antenna, is very complex, and losses degrade its performance. Such passive linear matching networks are not used in practice, as mentioned by Jakes [22, Sec. 5.3.1], although efforts are currently being made in this direction [14, 15].

Anyhow, the concept of a MIPMOP receiver front end, defined in Section 3.2, is not restricted to passive implementations. An active circuit may of course introduce coupling between several channels. An interesting candidate is the MIMO series-series feedback amplifier (MIMO-SSFA) [23, 24], which was initially introduced as an interface circuit for the reduction of crosstalk and echo in multiconductor interconnections. The possibility of designing a MIPMOP wireless receiver front end comprising a MIMO-SSFA, such as the one shown in Figure 8, was explained in [25].

Since the focus of this *Magazine* is not circuit theory, we omit the general definition of the MIMO-SSFA and the design procedure that may be used to obtain the desired characteristics of the MIPMOP receiver front end. In Figure 8, the low-noise MIPMOP amplifier is made of n uncoupled input-matching networks (C211 to C214 and L221 to L224), n uncoupled output matching networks (C521 to C524 and L511 to L514), and a MIMO-SSFA. The feedback network of the MIMO-SSFA only comprises the four inductors L411 to L414, coupled by mutual induction. This feedback network produces a negative feedback, creating coupling between the channels.

If mutual induction was not present, Figure 8 would represent four independent low-noise amplifiers with inductive source degeneration, capable of providing minimum noise figure and conjugate matching, simultaneously [16, 17]. Consequently, this low-noise MIPMOP amplifier requires no added circuit element, compared to the four independent low-noise amplifiers used in the conventional design of Figure 2.

8. An Example of a Design Using the MIMO-SSFA

This section applies to a circular array of four parallel half-wave dipole antennas (side-by-side configuration) for 1880 MHz,

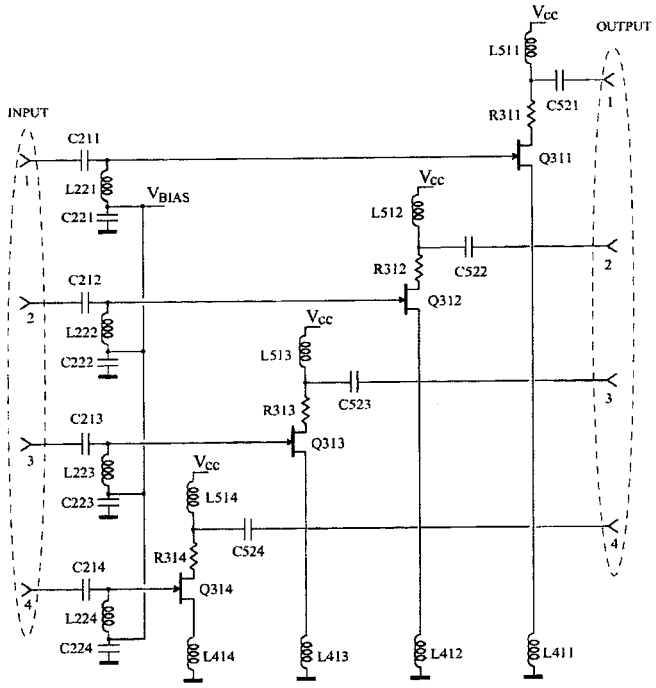

Figure 8. A low-noise MIPMOP amplifier comprising a MIMO-SSFA, four independent input-matching networks, and four independent output-matching networks.

presenting a $0.424\lambda = 27\,\text{mm}$ spacing between the nearest array elements. The impedance matrix of the antenna array is computed as

$$\mathbf{Z}_{ant} = \begin{pmatrix} 73.1 & 1.1-36.4j & -23.3-15.9j & 1.1-36.4j \\ 1.1-36.4j & 73.1 & 1.1-36.4j & -23.3-15.9j \\ -23.3-15.9j & 1.1-36.4j & 73.1 & 1.1-36.4j \\ 1.1-36.4j & -23.3-15.9j & 1.1-36.4j & 73.1 \end{pmatrix} \Omega \quad (17)$$

using the approach described in Section 2.1. For a zenith angle $\theta = \pi/2$, the open-circuit voltages are again 51 mV for an incident field of 1 V/m, and the matrix of the correlation coefficients, r_{ij}, of open-circuit voltages is

$$(r_{ij}) = \begin{pmatrix} 1.000 & -0.127 & -0.402 & -0.127 \\ -0.127 & 1.000 & -0.127 & -0.402 \\ -0.402 & -0.127 & 1.000 & -0.127 \\ -0.127 & -0.402 & -0.127 & 1.000 \end{pmatrix}. \quad (18)$$

8.1 The Case of a Conventional Front-End Design

For instance, let us assume that the array sees four uncoupled scalar loads of 73.0 Ω. The directional pattern is shown in Figure 9. The mean of the average powers oscillates between 3.3 μW and 4.2 μW as a function of the angle of arrival, φ. In the same field, a single dipole antenna in free space would deliver 4.4 μW to a 73.0 Ω load.

The correlation coefficients, r_{ij}, of antenna voltages are

$$(r_{ij}) = \begin{pmatrix} 1.000 & -0.209 & -0.215 & -0.209 \\ -0.209 & 1.000 & -0.209 & -0.215 \\ -0.215 & -0.209 & 1.000 & -0.209 \\ -0.209 & -0.215 & -0.209 & 1.000 \end{pmatrix}. \quad (19)$$

Again, we observe that the absolute value of a non-diagonal element of Equation (19) is sometimes higher and sometimes lower than the absolute value of the corresponding element of Equation (18).

8.2 The Case of a MIPMOP Front-End Design

We have designed a MIPMOP amplifier corresponding to the schematic diagram shown in Figure 8. It was designed in such a way that when each output port of the amplifier is connected to a grounded 50 Ω resistor, the amplifier provides an impedance $\mathbf{Z}_{LI}$ close to $\mathbf{Z}_{Sant}^*$ (Hermitian matching at the far end). This is for the case where the antennas are connected to the input of the amplifier using four 0.045-m-long transmission lines having propagation velocities of $0.5c_0$, characteristic impedances of 80 Ω, and attenuations of 2.0 dB/m, all at 1880 MHz. Our design is based on the characteristics of a commercially packaged low-noise pseudomorphic HEMT, and incorporates drain resistors shown in Figure 8, which provide resistive loading to improve stability. The resulting voltage gain matrix, $\mathbf{G}_V$, of the MIPMOP amplifier and $\mathbf{Z}_{SLI}$ are

$$\mathbf{G}_V = \begin{pmatrix} -2.80-3.32j & 0.06+0.86j & 0.24+0.37j & 0.06+0.86j \\ 0.06+0.86j & -2.80-3.32j & 0.06+0.86j & 0.24+0.37j \\ 0.24+0.37j & 0.06+0.86j & -2.80-3.32j & 0.06+0.86j \\ 0.06+0.86j & 0.24+0.37j & 0.06+0.86j & -2.80-3.32j \end{pmatrix} \quad (20)$$

$$\mathbf{Z}_{SLI} = \begin{pmatrix} 74.8+0.19j & 1.6+34.5j & -20.4+14.6j & 1.6+34.5j \\ 1.6+34.5j & 74.8+0.19j & 1.6+34.5j & -20.4+14.6j \\ -20.4+14.6j & 1.6+34.5j & 74.8+0.19j & 1.6+34.5j \\ 1.6+34.5j & -20.4+14.6j & 1.6+34.5j & 74.8+0.19j \end{pmatrix} \Omega \quad (21)$$

Although the design objective, $\mathbf{Z}_{LI} \approx \mathbf{Z}_{Sant}^*$, is not equivalent to $\mathbf{Z}_{ant} \approx \mathbf{Z}_{SLI}^*$ (Hermitian matching at the near end) because of losses in the transmission lines, a comparison of Equations (17) and (21) shows that Hermitian matching is almost reached between the antenna array and the near end of the transmission lines. Taking into account the voltage transfer matrix, $\mathbf{T}_V$, of the transmission lines obtained using Equation (43) of Appendix C, we compute the average powers delivered to each 50 Ω resistor and the mean of the average powers shown in Figure 10. The matrix of the correlation coefficients, r_{ij}, of the antenna voltages may be computed using

$$\langle \mathbf{V}_O \mathbf{V}_O^* \rangle = \mathbf{G}_T \langle \mathbf{V}_{antO} \mathbf{V}_{antO}^* \rangle \mathbf{G}_T^* \quad (22)$$

and

$$\mathbf{G}_T = \mathbf{G}_V \mathbf{T}_V \mathbf{Z}_{SLI} (\mathbf{Z}_{SLI} + \mathbf{Z}_{ANT})^{-1}, \quad (23)$$

where $\mathbf{V}_O$ is the column vector of the output voltages. We get

$$(r_{ij}) = \begin{pmatrix} 1.000 & -0.533 & 0.168 & -0.533 \\ -0.533 & 1.000 & -0.533 & 0.168 \\ 0.168 & -0.533 & 1.000 & -0.533 \\ -0.533 & 0.168 & -0.533 & 1.000 \end{pmatrix}. \quad (24)$$

According to Equation (24), the correlation of adjacent channels is not low, but acceptable. This is related to the fact that as shown in Figure 10, the main beam of a given channel corresponds to a strong sidelobe of the adjacent channel. A different design could correct this. However, this example clearly shows that a MIPMOP amplifier providing Hermitian matching does not necessarily provides a reduction of the correlation coefficients. This is quite different from an ideal lossless MIPMOP matching network providing bilateral Hermitian matching, which produces a perfect decorrelation. Other differences between the MIPMOP amplifier and a passive MIPMOP matching network are gain versus loss, and the number of additional circuit elements compared to a conventional design.

9. Conclusion

We have discussed some properties of an array of linear antennas when it is used as a multi-port device, as opposed to the classical theory of a antenna array used as a single-port device (which includes antennas having a single driven element, e.g., Yagi antennas, and arrays comprising multiple driven elements, e.g., using a beam-forming feed). We have shown that interesting properties are obtained when the front end of a receiver is a MIPMOP device, as opposed to multiple independent single-input-port and single-output-port devices. We have shown that a MIPMOP receiver front end may be based on an active circuit such as the MIMO-SSFA, and we provided an example in which this approach required no additional circuit elements compared to a conventional design.

The combination of a multi-port antenna and a MIPMOP front end is an active research area in which future developments are needed. For instance:

- We need to find out what the best design parameters for the MIPMOP circuits are, and how noise can be characterized, assessed, and minimized;
- We need more elaborate multi-port circuit-synthesis techniques, capable of providing wanted parameter values in a given bandwidth;
- We need practical models (e.g., equivalent circuits) for the impedance matrix of the antenna array in a given bandwidth for simple antennas, and for the more-complex antennas used in real applications (e.g., the PIFA antenna);
- We need to learn how we should specify a system made of the antenna array, the interconnections, and the MIPMOP front end for the best performance of the digital receiver (or transmitter);
- We need to discover how we could optimize the system made of the antenna array, the interconnections, and the MIPMOP front end, as a whole.

10. Appendix A: The Impedance Matrix of an Array of Dipole Antennas

Each dipole is parallel to the unit vector $\mathbf{e}_z$, and the electrical center of dipole number j has a position defined by the radius vector, $\mathbf{r}_j$. At the frequency f_0 for which the dipoles have a length close to a half wave, we assume [26, pp. 34-37] that each dipole presents a self-impedance equal to 73.13 Ω. Although a closed-form solution [27, eq. 8-73], based on the induced EMF method, is available for the computation of the mutual impedances of parallel dipoles, we found that the implementation of the cosine and sine integrals in *MathCAD* is such that accurate results are not obtained for all configurations. We therefore used a direct computation based on a closed-form formula for the fields and a numerical integration [27, eq. 8-68].

We assume that a plane wave of wave vector **k**, having a linear polarization along the unit vector **u**, impinges on the antenna array. Of course, we have $\mathbf{u}\bullet\mathbf{k}=0$. The open-circuit voltage, v_{antOj}, of antenna j is given by [26, p. 305; 28, p. 6-5]

$$v_{antOj} = H_{eff\,j} E_0 \exp\left(-j\mathbf{k}\bullet\mathbf{r}_j\right), \tag{25}$$

where E_0 is the magnitude of the incident electric field at the origin. The effective height, $H_{eff\,j}$, is

$$H_{eff\,j} = \frac{c_0}{\pi f_0}\frac{\cos\left(\frac{\pi}{2}\cos\theta\right)}{\sin\theta}\mathbf{u}\bullet\mathbf{e}_\theta, \tag{26}$$

where c_0 is the free-space light velocity, and $\mathbf{e}_\theta$ is the unit vector of the spherical coordinates corresponding to a partial derivative with respect to the zenith angle θ, that is to say, the angle between $\mathbf{e}_z$ and $-\mathbf{k}$.

11. Appendix B: Two-Dimensional Spatial Correlation Function

For a fixed receiver in a scattering-rich environment, let us use $\Gamma(d)$ to denote the correlation function between vertical electric fields E_z measured at two points having the same coordinates z, separated by the distance d. For this computation of a spatial correlation function, we will consider a two-dimensional Rayleigh channel, and follow the rigorous approach of De Doncker for the three-dimensional case [29]. The waves impinging the receiver are assumed to have equal energy (Rayleigh channel), and to propagate in the horizontal plane containing the antenna's position. Consequently, we have

$$E_z(\mathbf{r}) = \int_0^{2\pi} F(\theta) e^{-j\mathbf{k}\mathbf{r}} d\theta, \tag{27}$$

where **k** is the horizontal wave vector of a plane wave, θ is the azimuth of **k**, $F(\theta)$ is the complex plane-wave spectrum of E_z, and **r** is the horizontal radius vector of the antenna's position. Equation (27) corresponds to one realization of E_z. A given plane wave spectrum corresponds to each realization, and under these assumptions, $F(\theta)$ is a complex random function. Let us use $F_r(\theta)$ to denote the real part of $F(\theta)$, and $F_i(\theta)$ to denote the imaginary part of $F(\theta)$. For any azimuth θ, we have

$$\langle F(\theta)\rangle = \langle F_r(\theta)\rangle = \langle F_r(\theta)\rangle = 0. \tag{28}$$

Since two waves arriving from the azimuths θ_1 and θ_2 are uncorrelated and are supposed to have equal energy, we have

$$\langle F_r(\theta_1) F_r(\theta_2)\rangle = \langle F_i(\theta_1) F_i(\theta_2)\rangle = C\delta(\theta_1 - \theta_2), \tag{29}$$

where δ is the Dirac distribution and C is independent of the azimuths. Finally, the real and imaginary parts of $F(\theta)$ are assumed to be uncorrelated:

$$\left\langle F_r(\theta_1)F_i(\theta_2)\right\rangle = 0. \tag{30}$$

From these assumptions, we have

$$\begin{aligned}\left\langle |E_z(\mathbf{r})|^2 \right\rangle &= \int_0^{2\pi}\int_0^{2\pi} \left\langle F(\theta_1)\overline{F(\theta_2)}\right\rangle e^{-j(\mathbf{k}_1-\mathbf{k}_2)\mathbf{r}} d\theta_1 d\theta_2 \\ &= \int_0^{2\pi}\int_0^{2\pi} 2C\delta(\theta_1-\theta_2) e^{-j(\mathbf{k}_1-\mathbf{k}_2)\mathbf{r}} d\theta_1 d\theta_2 \\ &= 4\pi C.\end{aligned} \tag{31}$$

Since this quantity is assumed to be independent of the position, we obtain

$$C = \frac{\left\langle |E_z|^2 \right\rangle}{4\pi}. \tag{32}$$

We also have

$$\left\langle F(\theta_1)\overline{F(\theta_2)}\right\rangle = \frac{\left\langle |E_z|^2 \right\rangle}{2\pi}\delta(\theta_1-\theta_2). \tag{33}$$

Consequently, the correlation function between vertical electric fields E_z measured at $\mathbf{r}_1$ and $\mathbf{r}_2$ is

$$\begin{aligned}\left\langle E_z(\mathbf{r}_1)\overline{E_z(\mathbf{r}_2)}\right\rangle &= \int_0^{2\pi}\int_0^{2\pi} \left\langle F(\theta_1)\overline{F(\theta_2)}\right\rangle d\theta_1 d\theta_2 \\ &= \int_0^{2\pi}\int_0^{2\pi} \frac{\left\langle |E_z|^2 \right\rangle}{2\pi}\delta(\theta_1-\theta_2) e^{-j(\mathbf{k}_1\mathbf{r}_1-\mathbf{k}_2\mathbf{r}_2)} d\theta_1 d\theta_2 \\ &= \frac{\left\langle |E_z|^2 \right\rangle}{2\pi}\int_0^{2\pi} e^{-j\mathbf{k}(\mathbf{r}_1-\mathbf{r}_2)} d\theta.\end{aligned} \tag{34}$$

We have $\mathbf{k} = \cos\theta\mathbf{e}_x + \sin\theta\mathbf{e}_y$. We can choose $\mathbf{e}_x$ such that $\mathbf{r}_2 - \mathbf{r}_1 = d\mathbf{e}_x$ without loss of generality. We get

$$\begin{aligned}\Gamma(d) &= \frac{\left\langle |E_z|^2 \right\rangle}{2\pi}\int_0^{2\pi} e^{-jkd\cos\theta} d\theta \\ &= \frac{\left\langle |E_z|^2 \right\rangle}{\pi}\int_0^{\pi} \cos(kd\cos\theta) d\theta.\end{aligned} \tag{35}$$

Using Equation (9.1.18) of [30], we finally get

$$\Gamma(d) = \left\langle |E_z|^2 \right\rangle J_0(kd), \tag{36}$$

where J_0 is the Bessel function of the first kind of order 0. This is the result used in Jakes without proof [22, p. 329]. This result is compatible with experimental data [31, Sec. IV.C]. This result seems to have been first established by Clarke [32].

12. Appendix C. Transmission Lines Connected to the Antennas

We assume that each of the n antennas is connected to a two-conductor interconnection (for instance, a coaxial cable) behaving as a two-conductor transmission line, and that the interaction between these interconnections may be neglected. Let j be an integer greater than or equal to one, and less than or equal to n. Antenna number j is connected to the near-end lossless interconnection number j of length d_j, characteristic impedance z_{Cj}, phase velocity c_j, and attenuation constant α_j. The far end of interconnection number j is connected to the input port number j of a multiple-input-port and multiple-output-port (MIPMOP) amplifier comprising n input ports.

Let us define the characteristic impedance matrix, $\mathbf{Z}_C$, of the interconnections as

$$\mathbf{Z}_C = \mathrm{diag}_n\left(z_{C1},\ldots,z_{Cn}\right), \tag{37}$$

where $\mathrm{diag}_n(x_1,\ldots,x_n)$ denotes the diagonal matrix of size $n\times n$ of the components $x_1,\ldots,x_n$. Let us also define the transmission matrix, $\mathbf{T}$, of the interconnections as

$$\mathbf{T} = \mathrm{diag}_n\left(e^{-\left[\alpha_1+j\frac{2\pi f_0}{c_1}\right]d_1},\ldots,e^{-\left[\alpha_n+j\frac{2\pi f_0}{c_n}\right]d_n}\right). \tag{38}$$

We define $i_{ant\,j}$ as the current flowing into the near end of the positive conductor of interconnection number j; $i_{I\,j}$ as the current flowing into the positive terminal of port j of the MIPMOP amplifier; $v_{ant\,j}$ as the voltage between the near end of the positive and the negative conductors of interconnection number j; and $v_{I\,j}$ as the voltage between the positive and the negative terminals of port j of the MIPMOP amplifier. We also define $\mathbf{I}_{ant}$ as the column vector of the currents $i_{ant\,1},\ldots,i_{ant\,n}$; $\mathbf{I}_I$ as the column vector of the currents $i_{I1},\ldots,i_{In}$; $\mathbf{V}_{ant}$ as the column vector of the voltages $v_{ant\,1},\ldots,v_{ant\,n}$; and $\mathbf{V}_I$ as the column vector of the voltages $v_{I1},\ldots,v_{In}$.

As shown in Figure 1, let us use $\mathbf{Z}_{LI}$ to denote the impedance matrix looking into the MIPMOP amplifier, $\mathbf{Z}_{SLI}$ to denote the impedance matrix looking into the near end of the two-conductor interconnections, and $\mathbf{Z}_{Sant}$ to denote the impedance matrix looking into the far-end of the two-conductor interconnections. We have

$$\mathbf{V}_{ant} = E\,\mathbf{H}_{eff} - \mathbf{Z}_{ant}\mathbf{I}_{ant} = \mathbf{Z}_{SLI}\mathbf{I}_{ant}, \tag{39}$$

with

$$\begin{aligned}\mathbf{Z}_{SLI} = &\left\{\mathbf{1}_n + \mathbf{T}(\mathbf{Z}_{LI}-\mathbf{Z}_C)(\mathbf{Z}_{LI}+\mathbf{Z}_C)^{-1}\mathbf{T}\right\} \\ &\left\{\mathbf{1}_n - \mathbf{T}(\mathbf{Z}_{LI}-\mathbf{Z}_C)(\mathbf{Z}_{LI}+\mathbf{Z}_C)^{-1}\mathbf{T}\right\}^{-1}\mathbf{Z}_C,\end{aligned} \tag{40}$$

which can also be written as

$$\mathbf{Z}_{SLI} = \left\{\frac{\mathbf{T}+\mathbf{T}^{-1}}{2}\mathbf{Z}_{LI} - \frac{\mathbf{T}-\mathbf{T}^{-1}}{2}\mathbf{Z}_C\right\} \left\{\frac{\mathbf{T}+\mathbf{T}^{-1}}{2}\mathbf{Z}_C - \frac{\mathbf{T}-\mathbf{T}^{-1}}{2}\mathbf{Z}_{LI}\right\}^{-1}\mathbf{Z}_C. \quad (41)$$

Consequently, $\mathbf{V}_{ant}$ and $\mathbf{I}_{ant}$ are given by

$$\begin{cases}\mathbf{V}_{ant} = \mathbf{Z}_{SLI}\left(\mathbf{Z}_{ant}+\mathbf{Z}_{SLI}\right)^{-1} E\,\mathbf{H}_{eff} \\ \mathbf{I}_{ant} = \left(\mathbf{Z}_{ant}+\mathbf{Z}_{SLI}\right)^{-1} E\,\mathbf{H}_{eff}\end{cases}. \quad (42)$$

Using Equation (41), we easily obtain

$$\mathbf{V}_I = \mathbf{Z}_{LI}\left\{\frac{\mathbf{T}+\mathbf{T}^{-1}}{2}\mathbf{Z}_C - \frac{\mathbf{T}-\mathbf{T}^{-1}}{2}\mathbf{Z}_{LI}\right\}^{-1} \mathbf{Z}_C\left(\mathbf{Z}_{ant}+\mathbf{Z}_{SLI}\right)^{-1} E\,\mathbf{H}_{eff},$$
$$\mathbf{I}_I = \left\{\frac{\mathbf{T}+\mathbf{T}^{-1}}{2}\mathbf{Z}_C - \frac{\mathbf{T}-\mathbf{T}^{-1}}{2}\mathbf{Z}_{LI}\right\}^{-1} \mathbf{Z}_C\left(\mathbf{Z}_{ant}+\mathbf{Z}_{SLI}\right)^{-1} E\mathbf{H}_{eff}. \quad (43)$$

Of course, the impedance matrix, $\mathbf{Z}_{Sant}$, looking into the far end of the two-conductor interconnections is given by

$$\mathbf{Z}_{Sant} = \left\{\mathbf{1}_n + \mathbf{T}\left(\mathbf{Z}_{ant}-\mathbf{Z}_C\right)\left(\mathbf{Z}_{ant}+\mathbf{Z}_C\right)^{-1}\mathbf{T}\right\} \left\{\mathbf{1}_n - \mathbf{T}\left(\mathbf{Z}_{ant}-\mathbf{Z}_C\right)\left(\mathbf{Z}_{ant}+\mathbf{Z}_C\right)^{-1}\mathbf{T}\right\}^{-1}\mathbf{Z}_C, \quad (44)$$

which can also be written as

$$\mathbf{Z}_{Sant} = \left\{\frac{\mathbf{T}+\mathbf{T}^{-1}}{2}\mathbf{Z}_{ant} - \frac{\mathbf{T}-\mathbf{T}^{-1}}{2}\mathbf{Z}_C\right\} \left\{\frac{\mathbf{T}+\mathbf{T}^{-1}}{2}\mathbf{Z}_C - \frac{\mathbf{T}-\mathbf{T}^{-1}}{2}\mathbf{Z}_{ant}\right\}^{-1}\mathbf{Z}_C. \quad (45)$$

In the special case where the impedance matrix, $\mathbf{Z}_{LI}$, looking into the MIPMOP amplifier is diagonal, the input ports of this MIPMOP amplifier look like the input of n uncoupled amplifiers. In this case, all matrices in Equations (40) and (41) commute. Of course, matching is obtained for $\mathbf{Z}_{LI} = \mathbf{Z}_C$.

13. References

1. M. D. Migliore, "An Intuitive Electromagnetic Approach to MIMO Communication Systems," *IEEE Antennas and Propagation Magazine*, **48**, 3, June 2006, pp. 128-137.

2. J. D. Kraus, *Antennas*, New York, McGraw-Hill, 1950.

3. R. S. Adve and T. K. Sarkar, "Compensation for the Effects of Mutual Coupling on Direct Data Domain Adaptive Algorithms," *IEEE Transactions on Antennas and Propagation*, **AP-48**, 1, January 2000, pp. 86-94.

4. C. A. Desoer, "The Maximum Power Transfer Theorem for *n*-Ports," *IEEE Trans. Circuit Theory*, **20**, 3, May 1973, pp. 328-330.

5. M. Vidyasagar, "Maximum Power Transfer in *n* Ports with Passive Loads," *IEEE Trans. Circuit Theory*, **21**, 3, May 1974, pp. 327-330.

6. R. Vaughan and N. Scott, "Closely Spaced Terminated Monopoles for Vehicular Diversity Antennas," 1992 IEEE International Symposium on Antennas and Propagation *Digest*, **2**, July 18-25, 1992, pp. 1093-1096.

7. G. L. Stüber et al, "Broadband MIMO-OFDM Wireless Communications," *Proceedings of the IEEE*, **92**, 2, February 2004, pp. 271-294.

8. J. Mietzner and P. A. Hoeher, "Boosting the Performance of Wireless Communication Systems: Theory and Practice of Multiple-Antenna Techniques," *IEEE Commun. Mag.*, **42**, 10, October 2004, pp. 40-47.

9. M. A. Jensen and J. W. Wallace, "A Review of Antennas and Propagation for MIMO Wireless Communications," *IEEE Transactions on Antennas and Propagation*, **AP-52**, 11, November 2004, pp. 2810-2824.

10. R. A. Speciale, "Advanced Design of Phased-Array Beam-Forming Networks," *IEEE Transactions on Antennas and Propagation*, **AP-38**, 4, August 1996, pp. 22-34.

11. J. W. Wallace and M. A. Jensen, "Termination-Dependent Diversity Performance of Coupled Antennas: Network Theory Analysis," *IEEE Transactions on Antennas and Propagation*, **AP-52**, 1, January 2004, pp. 98-105.

12. J. W. Wallace and M. A. Jensen, "Mutual Coupling in MIMO Wireless Systems: A Rigorous Network Theory Analysis," *IEEE Trans. Wireless Commun.*, **3**, 4, July 2004, pp. 1317-1325.

13. S. Stein, "On Cross Coupling in Multiple-Beam Antennas," *IRE Transactions on Antennas and Propagation*, **AP-10**, 5, September 1962, pp. 548-557.

14. J. Weber, C. Volmer, K. Blau, R. Stephan, M. A. Hein, "Miniaturisation of Antenna Arrays for Mobile Communications," *Proc. 35th European Microwave Conf.*, Paris, France, October 2005, pp. 1173-1176.

15. J. Weber, C. Volmer, K. Blau, R. Stephan, M. A. Hein, "Miniaturized Antenna Arrays Using Decoupling Networks with Realistic Elements," *IEEE Trans. Microwave Theory Tech.*, **MTT-54**, 6, June 2006, pp. 2733-2740.

16. J. Engberg, "Simultaneous Input Power Match and Noise Optimization Using Feedback," *Dig. Tech. Pap. Fourth European Microwave Conference*, Montreux, September 1974, pp. 385-389.

17. R. E. Lehmann and D. D. Heston, "X-Band Monolithic Series Feedback LNA," *IEEE Trans. Microwave Theory Tech.*, **MTT-33**, 12, December 1985, pp. 1560-1566.

18. K. Boyle, "Radiation Patterns and Correlation of Closely Spaced Linear Antennas," *IEEE Transactions on Antennas and Propagation*, **AP-50**, 8, August 2002, pp. 1162-1165.

19. G. Gonzalez, *Microwave Transistor Amplifiers – Analysis and Design, Second Edition*, Upper Saddle River, NJ, Prentice Hall, 1997.

20. A. Pacaud, *Électronique radiofréquence*, Paris, Ellipses, 2000.

21. I. Hickman, *Practical Radio-Frequency Handbook, Third Edition*, Oxford, Newnes, 2002.

22. W. C. Jakes, *Microwave Mobile Communications*, New York, Wiley-Interscience, 1994.

23. F. Broydé and E. Clavelier, "A Simple Method for Transmission with Reduced Crosstalk and Echo," *Proc. of the 13th IEEE Int. Conf. on Electronics, Circuits and Systems*, ICECS 2006, December 10-13, 2006, Nice, France, pp. 684-687.

24. F. Broydé and E. Clavelier, "MIMO Series-Series Feedback Amplifiers," to appear in *IEEE Transactions on Circuits and Systems II*.

25. F. Broydé and E. Clavelier, "Multiple-Input-Port and Multiple-Output-Port Amplifier for Wireless Receivers," *Proc. of the SAME 2007 Forum*, Sophia-Antipolis, France, October 3-4, 2007; available at http://www.eurexcem.com.

26. R. E. Collin, *Antennas and Radiowave Propagation, International Edition*, New York, McGraw-Hill, 1985.

27. C. A. Balanis, *Antenna Theory, Analysis and Design, Second Edition*, New York, John Wiley & Sons, Inc., 1997.

28. Y. T. Lo and S.W. Lee, *Antenna Handbook, Volume II, Antenna Theory*, New York, Van Nostrand Reinhold, 1993.

29. Ph. De Doncker, "Spatial Correlation Functions for Fields in Three-Dimensional Rayleigh Channels," *Progress in Electromagnetic Research*, PIER 40, 2003, pp. 55-69.

30. M. Abramowitz and I. A. Stegun, *Handbook of Mathematical Functions*, New York, Dover, 1965.

31. J. W. Wallace, M. A. Jensen, A. L. Swindlehurst, and B. D. Jeffs, "Experimental Characterization of the MIMO Wireless Channel: Data Acquisition and Analysis," *IEEE Trans. Wireless Commun.*, **2**, 2, March 2003, pp. 335-343.

32. R. H. Clarke, "A Statistical Theory of Mobile-Radio Reception," *Bell Syst. Tech. Journal*, July-August 1968, pp. 957-1000.